Epidermal Electronics

Dae-Hyeong Kim,[1]* Nanshu Lu,[1]* Rui Ma,[2]* Yun-Soung Kim,[1] Rak-Hwan Kim,[1] Shuodao Wang,[3] Jian Wu,[3] Sang Min Won,[1] Hu Tao,[4] Ahmad Islam,[1] Ki Jun Yu,[1] Tae-il Kim,[1] Raeed Chowdhury,[2] Ming Ying,[1] Lizhi Xu,[1] Ming Li,[3,6] Hyun-Joong Chung,[1] Hohyun Keum,[1] Martin McCormick,[2] Ping Liu,[5] Yong-Wei Zhang,[5] Fiorenzo G. Omenetto,[4] Yonggang Huang,[3] Todd Coleman,[2] John A. Rogers[1]†

We report classes of electronic systems that achieve thicknesses, effective elastic moduli, bending stiffnesses, and areal mass densities matched to the epidermis. Unlike traditional wafer-based technologies, laminating such devices onto the skin leads to conformal contact and adequate adhesion based on van der Waals interactions alone, in a manner that is mechanically invisible to the user. We describe systems incorporating electrophysiological, temperature, and strain sensors, as well as transistors, light-emitting diodes, photodetectors, radio frequency inductors, capacitors, oscillators, and rectifying diodes. Solar cells and wireless coils provide options for power supply. We used this type of technology to measure electrical activity produced by the heart, brain, and skeletal muscles and show that the resulting data contain sufficient information for an unusual type of computer game controller.

Physiological measurement and stimulation techniques that exploit interfaces to the skin have been of interest for more than 80 years, beginning in 1929 with electroencephalography from the scalp (1–3). Nearly all associated device technologies continue, however, to rely on conceptually old designs. Typically, small numbers of bulk electrodes are mounted on the skin via adhesive tapes, mechanical clamps or straps, or penetrating needles, often mediated by conductive gels, with terminal connections to separate boxes that house collections of rigid circuit boards, power supplies, and communication components (4–9). These systems have many important capabilities, but they are poorly suited for practical application outside of research labs or clinical settings because of difficulties in establishing long-lived, robust electrical contacts that do not irritate the skin and in achieving integrated systems with overall sizes, weights, and shapes that do not cause discomfort during prolonged use (8, 9). We introduce a different approach, in which the electrodes, electronics, sensors, power supply, and communication components are configured together into ultrathin, low-modulus, lightweight, stretchable

"skin-like" membranes that conformally laminate onto the surface of the skin by soft contact, in a manner that is mechanically invisible to the user, much like a temporary transfer tattoo.

Materials, mechanics, and design strategies. A demonstrative platform is shown in Fig. 1, integrating a collection of multifunctional sensors (such as temperature, strain, and electrophysiological), microscale light-emitting diodes (LEDs), active/passive circuit elements (such as transistors, diodes, and resistors), wireless power coils, and devices for radio frequency (RF) communications (such as high-frequency inductors, capacitors, oscillators, and antennae), all integrated on the surface of a thin (~30 μm), gas-permeable elastomeric sheet based on a modified polyester (BASF, Ludwigshafen, Germany) with low Young's modulus (~60 kPa) (fig. S1A). The devices and interconnects exploit ultrathin layouts (<7 μm), neutral mechanical plane configurations, and optimized geometrical designs. The active elements use established electronic materials, such as silicon and gallium arsenide, in the form of filamentary serpentine nanoribbons and micro- and nanomembranes. The result is a high-performance system that offers reversible, elastic responses to large strain deformations with effective moduli (<150 kPa), bending stiffnesses (<1 nN m), and areal mass densities (<3.8 mg/cm^2) that are orders of magnitude smaller than those possible with conventional electronics or even with recently explored flexible/stretchable device technologies (10–19). Water-soluble polymer sheets [polyvinyl alcohol (PVA) (Aicello, Toyohashi, Japan); Young's modulus, ~1.9 GPa; thickness, ~50 μm (fig. S1B)] serve as temporary supports for manual mounting of these systems on the skin in an overall construct that is directly analogous to that of a temporary transfer tattoo. The image in Fig. 1B, top, is of a device similar to the one in Fig. 1A, after mounting it onto the skin by washing away the PVA and then partially

peeling the device back with a pair of tweezers. When completely removed, the system collapses on itself because of its extreme deformability and skin-like physical properties, as shown in Fig. 1B, bottom (movie S1). The schematic illustration in the inset shows an approximate cross-sectional layout.

These mechanical characteristics lead to robust adhesion to the skin via van der Waals forces alone, without any mechanical fixturing hardware or adhesive tapes. The devices impose negligible mechanical or mass loading (typical total mass of ~0.09 g), as is evident from the images of Fig. 1C, which show the skin deforming freely and reversibly, without any apparent constraints in motion due to the devices. Electronics in this form can even be integrated directly with commercial temporary transfer tattoos as a substrate alternative to polyester or PVA. The result, shown in Fig. 1D, is of possible interest as a way to conceal the active components and to exploit low-cost materials (the substrate, adhesives, and backing layers) already developed for temporary transfer tattoos (movie S1). Potential uses include physiological status monitoring, wound measurement/treatment, biological/chemical sensing, human-machine interfaces, covert communications, and others.

Understanding the mechanics of this kind of device, the mechanophysiology of the skin, and the behavior of the coupled abiotic-biotic system are all important. For present purposes, the skin can be approximated as a bilayer, consisting of the epidermis (modulus, 140 to 600 kPa; thickness, 0.05 to 1.5 mm) and the dermis (modulus, 2 to 80 kPa; thickness, 0.3 to 3 mm) (20–23). This bilayer exhibits linear elastic response to tensile strains ≲15%, which transitions to nonlinear behavior at higher strains, with adverse, irreversible effects beyond 30% (24). The surface of the skin has wrinkles, creases, and pits with amplitudes and feature sizes of 15 to 100 μm (25) and 40 to 1000 μm (26), respectively. The devices described here (Fig. 1) have moduli, thicknesses, and other physical properties that are well matched to the epidermis, with the ability to conform to the relief on its surface. We therefore refer to this class of technology as an "epidermal electronic system" (EES).

Macroscopically, an EES on skin can be treated as a thin film on an epidermis–dermis bilayer substrate. Microscopically, the sizes of the individual electronic components and interconnects are comparable with those of relief features on the skin and therefore must be considered explicitly. We began by considering aspects of adhesion, in the macroscopic limit. Globally, detachment can occur in either tension or compression because of interfacial cracks that initiate at the edges or the central regions of the EES, respectively. Low effective moduli and small thicknesses minimize the deformation-induced stored elastic energy that drives both of these failure modes. Analytical calculation (27) shows that

[1]Department of Materials Science and Engineering, Beckman Institute for Advanced Science and Technology, and Frederick Seitz Materials Research Laboratory, University of Illinois at Urbana-Champaign, Urbana, IL 61801, USA. [2]Department of Electrical and Computer Engineering, Coordinated Science Laboratory, University of Illinois at Urbana-Champaign, Urbana, IL 61801, USA. [3]Department of Mechanical Engineering and Department of Civil and Environmental Engineering, Northwestern University, Evanston, IL 60208, USA. [4]Department of Biomedical Engineering, Tufts University, Medford, MA 02155, USA. [5]Institute of High Performance Computing, 1 Fusionopolis Way, #16-16 Connexis, 138632, Singapore. [6]State Key Laboratory of Structural Analysis for Industrial Equipment, Dalian University of Technology, Dalian 116024, China.

*These authors contributed equally to this work.
†To whom correspondence should be addressed. E-mail: jrogers@uiuc.edu

compared with silicon chips (thickness of ~1 mm) and sheets of polyimide (thickness of ~75 μm), the driving forces for delamination of the EES/skin interface are reduced by more than seven and four orders of magnitude, respectively. Measurements and theoretical calculations (27) shown in Fig. 2A explore the relevant scaling behaviors in structures that provide simplified, macroscopic models of EES/skin. The experiments use sheets of polyester (~2 mm thick) for the skin and films of poly(dimethylsiloxane) (PDMS) (Dow Corning, Midland, USA) for the EES. The critical delamination strain is plotted in Fig. 2A as a function of PDMS thickness for two different formulations: one with a modulus of 19 kPa (50:1) and

the other 145 kPa (30:1) (fig. S1C). The results, both theory and experiment, confirm that reducing the modulus and thickness lowers the driving forces for interface delamination for a given applied strain (bending or stretching) without lower bound.

The mechanical properties of the EES depend on the effective modulus and thickness of both the circuits and sensors and the substrate. In samples such as those in Fig. 1, the properties of the active components and interconnects can dominate the mechanics of the overall system. The in-plane layouts and materials of this layer are therefore key design parameters. Recent work in stretchable electronics establishes that the

overall range of deformability can be optimized in systems composed of active devices joined together in open-mesh structures by non-coplanar interconnects in neutral mechanical plane configurations, in which elastomers with relatively large moduli (2 to 10 MPa) and thicknesses (millimeters to centimeters) serve as substrates (13, 14). For EES, the effective modulus (E_{EES}) and bending stiffness ($\overline{EI}_{EES}$), rather than the range of stretchability, are paramount. These requirements demand alternative designs and choices of materials. If we assume that the effective moduli of the individual devices (for example, Young's modulus ~160 GPa for Si and ~90 GPa for GaAs) are much higher than those of the
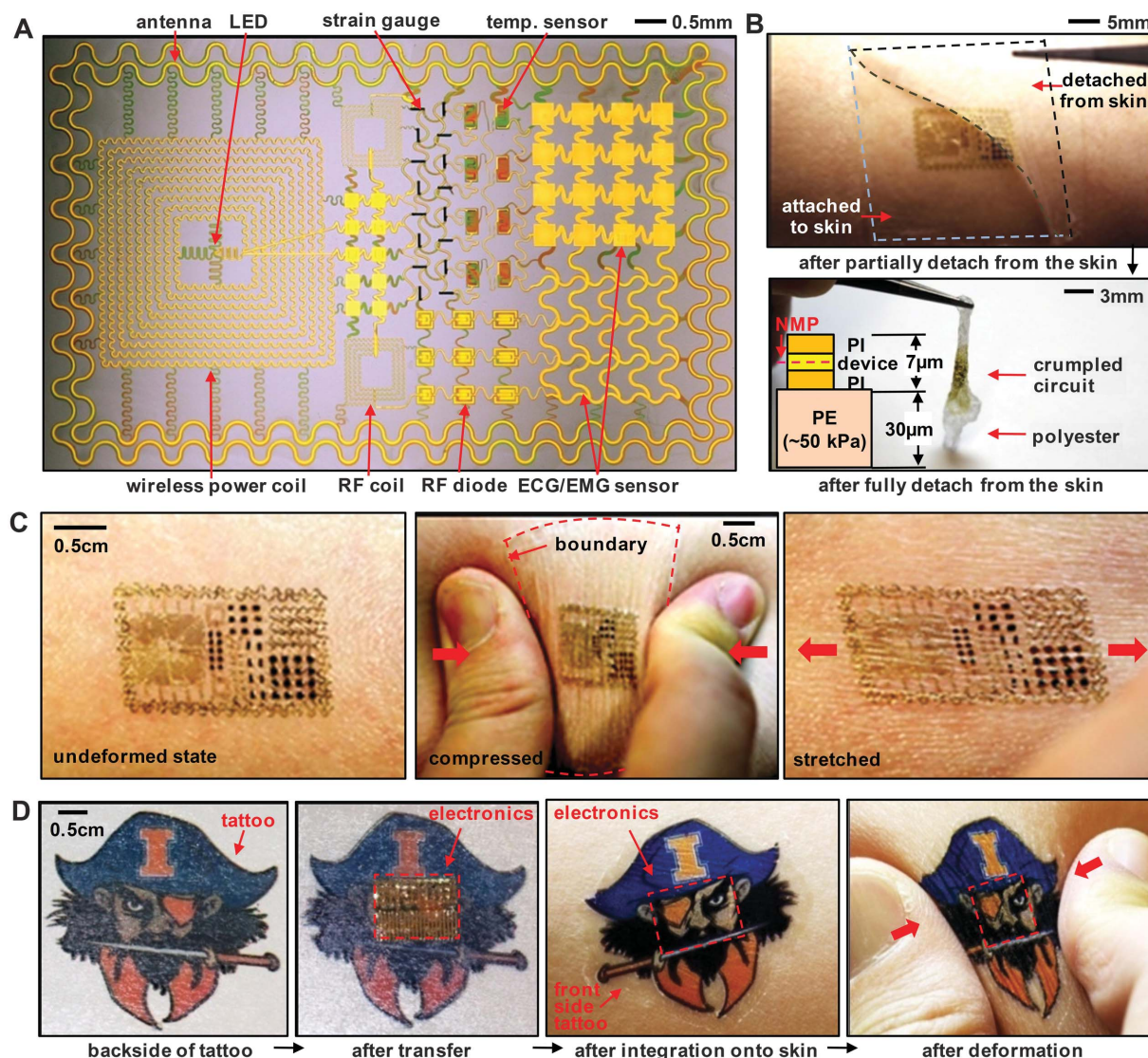

Fig. 1. (**A**) Image of a demonstration platform for multifunctional electronics with physical properties matched to the epidermis. Mounting this device on a sacrificial, water-soluble film of PVA, placing the entire structure against the skin, with electronics facing down, and then dissolving the PVA leaves the device conformally attached to the skin through van der Waals forces alone, in a format that imposes negligible mass or mechanical loading effects on the skin. (**B**) EES partially (top) and fully (bottom) peeled away from the skin. (Inset) A representative cross-sectional illustration of the struc-ture, with the neutral mechanical plane (NMP) defined by a red dashed line. (**C**) Multifunctional EES on skin: undeformed (left), compressed (middle), and stretched (right). (**D**) A commercial temporary transfer tattoo provides an alternative to polyester/PVA for the substrate; in this case, the system includes an adhesive to improve bonding to the skin. Images are of the backside of a tattoo (far left), electronics integrated onto this surface (middle left), and attached to skin with electronics facing down in undeformed (middle right) and compressed (far right) states.

interconnects and that the interconnected device components (rather than the substrate) dominate the mechanics, then we can write the approximate expression $E_{EES} = E_{int}(1 + L_d/L_s)$, where E_{int} is the effective modulus of the interconnects, L_d is the characteristic device size, and L_s is the distance between devices, as illustrated in fig. S1D. The value of E_{EES} can be minimized by reducing E_{int} and L_d/L_s. For the former, thin narrow interconnect lines formed into large-amplitude "filamentary serpentine" (FS) shapes represent effective designs. For the latter, ultrathin active devices that adopt similar FS layouts and continuously integrate with FS interconnects reduce the effective value of L_d to zero. The value of $\overline{EI}_{EES}$ decreases rapidly with the thicknesses of the devices, interconnects, and substrate. An ultrathin FS construct is shown in Fig. 2B, left, with a cross-sectional schematic illustration as an inset. Results of tensile testing

(Fig. 2B, right) indicate that such FS-EES samples (Fig. 2B, left) achieve E_{EES} (~140 kPa) and $\overline{EI}_{EES}$ (~0.3 nNm) (27) that are comparable with the epidermis and more than one and five orders of magnitude smaller than previously reported stretchable electronic devices, respectively (28). Furthermore, highly repeatable loading and unloading stress-strain curves up to strains of 30% demonstrate purely elastic responses, with maximum principal strains in the metals that are less than ~0.2% (fig. S1E). Calculations yield effective tensile moduli (Fig. 2B, right), with excellent correspondence to experiment. Such FS layouts can maintain nearly 20% areal contact of active elements with the skin, for effective electrical interfaces. In certain applications, layouts that involve some combination of FS geometries and device islands (L_d not equal to zero) connected by FS interconnects (Fig. 1 and fig. S1F) can be used, with expected consequences on the local

mechanics (fig. S1G). In both options, suitable designs lead to mechanical and adhesive properties that allow conformal adhesion to the skin and minimal loading effects (Fig. 2C). Without optimized layouts, we observed delamination under similar conditions of deformation (fig. S1H), which is consistent with the fracture modes illustrated in Fig. 2A.

For many uses of EES, physical coupling of devices to the surface of the skin is important. Confocal micrographs of EES mounted on pig skin appear in Fig. 2, D and E, as well as fig. S2C [dye information and bare pig skin confocal micrographs are shown in fig. S2, A and B, respectively; sample preparation and imaging procedures can be found in (27)]. With FS structures, the results show remarkably conformal contact, not only at the polyester regions of the EES but also at the FS elements (Fig. 2, D and E). Similar behavior was obtained, but in a less ideal
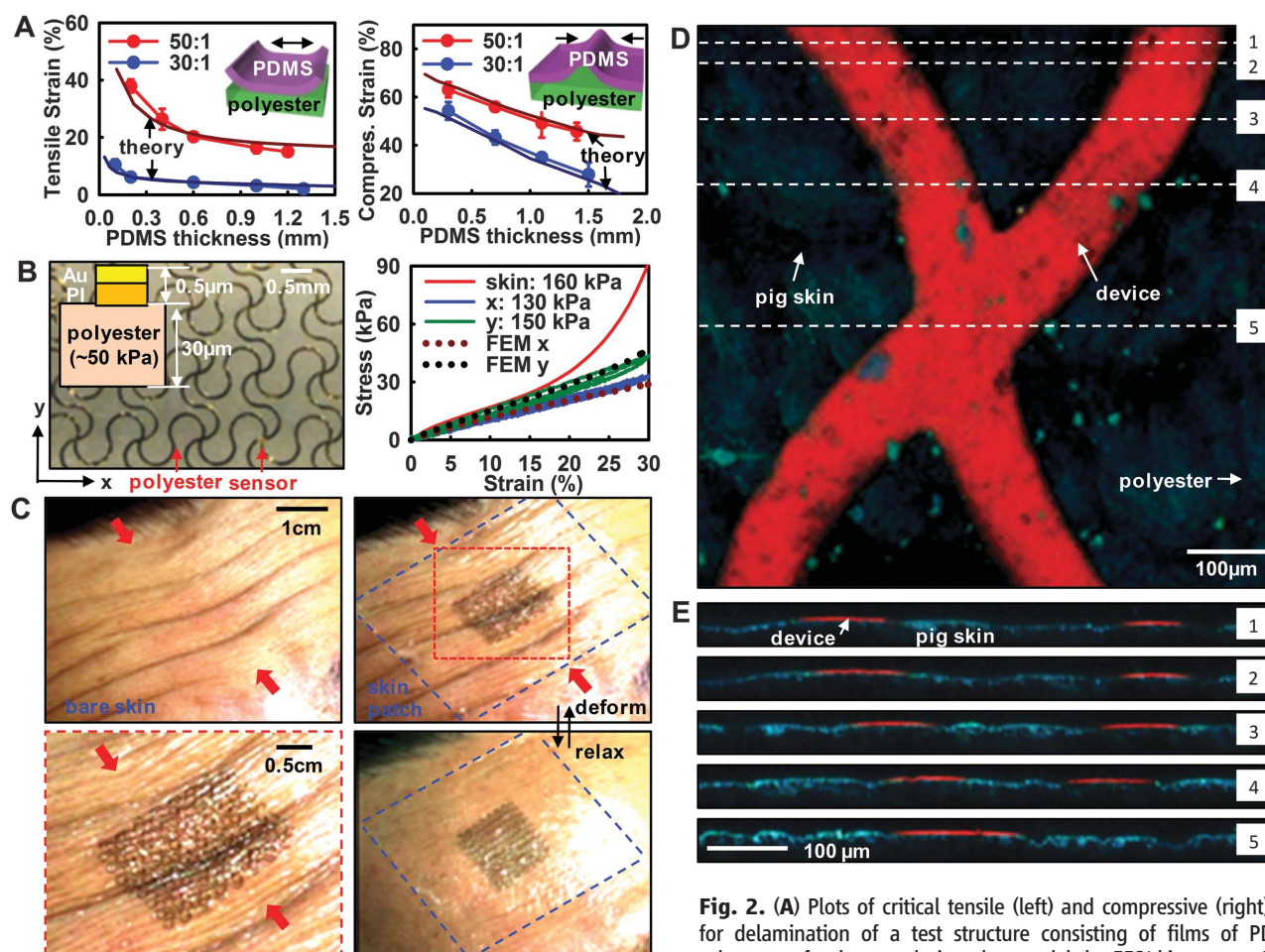

Fig. 2. (A) Plots of critical tensile (left) and compressive (right) strains for delamination of a test structure consisting of films of PDMS on substrates of polyester, designed to model the EES/skin system. Data for formulations of PDMS with two different moduli are shown (red, 19 kPa; blue, 145 kPa). The critical strains increase as the PDMS thickness and modulus decrease, which is consistent with modeling results (lines). **(B)** Optical micrograph of an EES with FS design (left). The plot (right) shows the stress-strain data from uniaxial tensile measurements for two orthogonal directions. Data collected from a sample of pig skin are also presented. The dotted lines correspond to calculations performed with finite element modeling. **(C)** Skin of the forehead before (top left) and after the mounting of a representative FS-EES, at various magnifications and states of deformation. The dashed blue boxes at right highlight the outer boundary of the device. The red arrows indicate the direction of compressive strains generated by a contraction of facial muscles. The red dashed box at the top right corresponds to the field of view of the image in the bottom left. **(D)** Confocal microscope image (top view) at the vicinity of the contacting interface between an FS-EES laminated on a sample of pig skin. The FS structure and the skin are dyed with red and blue fluorophores, respectively. **(E)** Cross-sectional confocal images at locations corresponding to the numbered, white dashed lines shown in the top-view frame above.

fashion (fig. S2C), with layouts that incorporate device islands. These observations are consistent with analytical mechanics treatments that use macroscopic models of the EES and account for microscopic structures on the skin (27). Related calculations suggest that spontaneous pressures created by surface interactions are ~10 kPa (fig. S10B), which is below the sensitivity of human skin (~20 kPa) (29) but still sufficient to offer reasonable adhesion. Microscopic models indicate that these interactions generate compressive forces (per unit length) of ~−0.1 N/m for each FS strip (27). Improved bonding can be achieved by using adhesives that are built into platforms for temporary transfer tattoos, as in Fig. 1D.

Multifunctional operation. A key capability of EES is in monitoring electrophysiological (EP) processes related to activity of the brain [electroencephalograms (EEGs)], the heart [electrocardiograms (ECGs)] and muscle tissue [electromyograms (EMGs)]. Amplified sensor electrodes that incorporate silicon metal oxide semiconductor field effect transistors (MOSFETs) in circuits in which all components adopt FS designs provide devices for this purpose. Here, the gate of a FS-MOSFET connects to an extended FS electrode for efficient coupling to the body potential (Fig.

3A; the inset shows an analogous design based on a rectangular device island and FS interconnects) via contact with the skin in a common-source amplifier configuration (Fig. 3B, left). The measured frequency response at different input capacitances (C_{IN}) is indicated in Fig. 3B, right, and is in quantitative agreement with circuit simulations (fig. S3, A and B). The value of C_{IN} is determined by a series combination of capacitances of the gate electrode, the encapsulating PI, and junction between the gate electrode and the body surface. The bandwidth matches requirements for high-performance EP recording. A typical layout for this purpose includes four amplified channels, each comprising a FS-MOSFET, a silicon-based FS resistor, and an FS electrode. One channel provides a reference, whereas the others serve as sites for measurement. Results of demonstration experiments appear subsequently.

Many other classes of semiconductor devices and sensors are also possible in EES, including resistance-based temperature sensors built with meander electrodes of Pt (Fig. 3C, left, and fig. S3C), in-plane strain gauges based on carbon-black-doped silicones (Fig. 3C, right, and fig. S3D), LEDs and photodetectors based on AlInGaP (for possible use in optical characteri-

zation of the skin/biofluids) (Fig. 3D, left, and fig. S3, E to G), and silicon FS photovoltaic cells (Fig. 3D, right). Such cells can generate a few tens of microwatts (fig. S3H); increasing the areas or areal coverages can improve the output, but not without compromises in size and mechanics. Wireless powering via inductive effects represents an appealing alternative. An example of an FS inductive coil connected to a microscale InGaN LED is shown in Fig. 3E, with electromagnetic modeling of its RF response. The resonance frequency (~35 MHz) matches that of a separately located transmission coil powered by an external supply. Voltage and current outputs in the receiver are sufficient to operate the microscale LEDs remotely, as shown in Fig. 3E. Such coils provide power directly in this example; they can also conceivably be configured to charge future classes of EES-integrated storage capacitors or batteries.

Examples of various RF components of the type needed for wireless communications or for scavenging RF energy are presented in Fig. 3, F and G. Shown in Fig. 3F is an optical image of silicon PIN diode (left) and its small-signal scattering parameters (fig. S3K), indicating insertion loss (S21 in forward condition) of <6 dB and isolation (S21 in reverse condition) of >15 dB
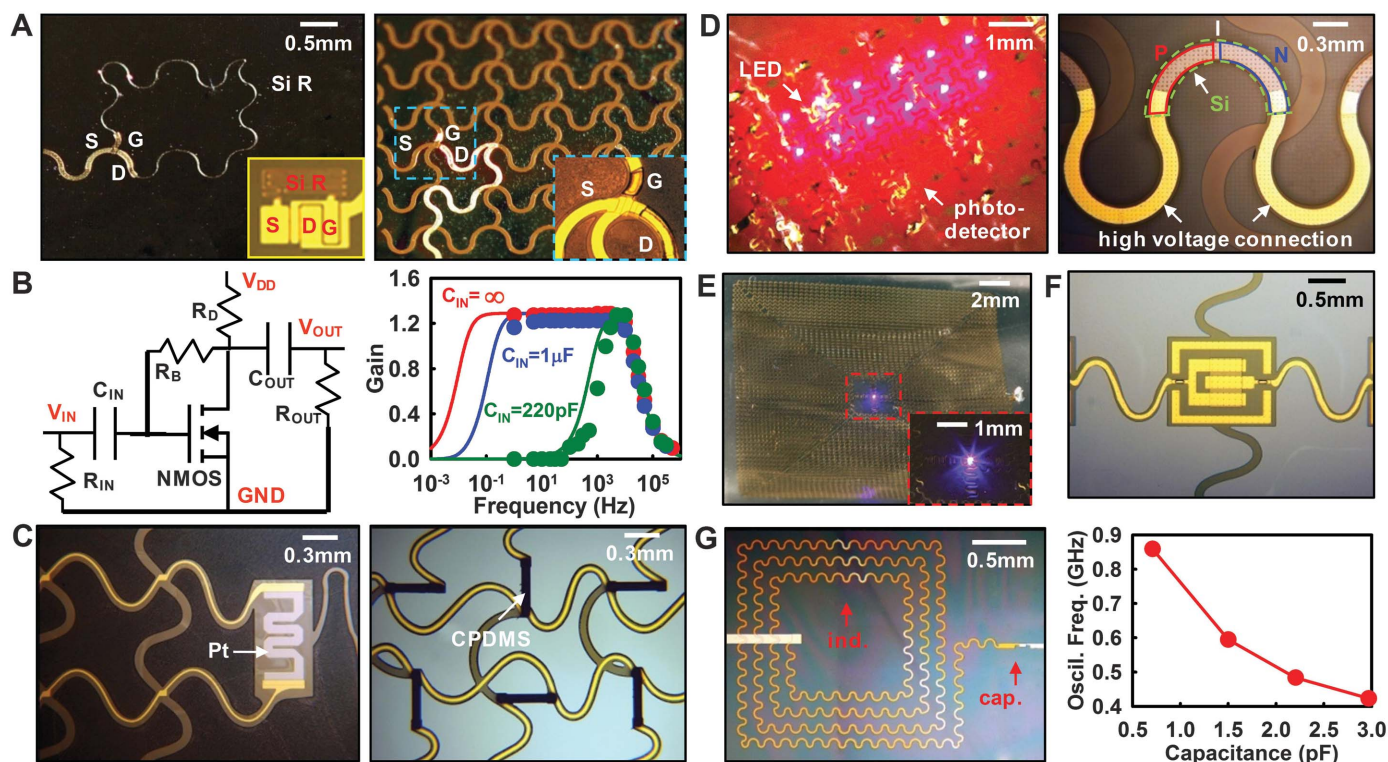

Fig. 3. (**A**) Optical micrographs of an active electrophysiological (EP) sensor with local amplification, as part of an FS-EES. (Left) The source, drain, and gate of a silicon MOSFET and a silicon feedback resistor before connection to sensor electrodes, all in FS layouts. (Inset) Similar device with island design. (Right) The final device, after metallization for the interconnects and sensor electrodes, with magnified view (inset). (**B**) Circuit diagram for the amplified EP sensor shown above (left). (Right) Measured and simulated frequency response for different input capacitance ($C_{IN} = \infty$, 1μF, 220pF). (**C**) Optical micrograph of a temperature sensor that uses a platinum resistor with FS interconnects (left) and a strain gauge that uses electrically conductive silicone (CPDMS; right). (**D**) Image of an array of microscale AlInGaP LEDs and photodetectors, in an interconnected array integrated on skin, under compressive deformation (left) and of a FS silicon solar cell (right). (**E**) Image of a FS wireless coil connected to a microscale InGaN LED, powered by inductive coupling to a separate transmission coil (not in the field of view). (**F**) Optical micrograph of a silicon RF diode. (**G**) Optical micrograph of an interconnected pair of FS inductors and capacitors designed for RF operation (left). The graph at right shows resonant frequencies for LC oscillators built with different FS capacitors.

for frequencies of up to 2 GHz. Examples of FS inductors and capacitors and their RF responses appear in Fig. 3G and fig. S3L. Connecting pairs of such devices yields oscillators with expected resonant frequencies (Fig. 3G, right). A notable behavior is that the response varies with the state of deformation because of the dependence of the RF inductance on geometry. For example, at tensile strains of ~12% the resonance frequency shifts by ~30% (fig. S3, I and J). Such effects, which also appear in the wireless power coils but not in the other devices of Fig. 3, will influence the behavior of antenna structures and certain related RF components. These issues must be considered explicitly in EES design and modes of operation.

Systems for electrophysiological recording. EES configured for measuring ECG, EMG, and EEG in conformal, skin-mounted modes without conductive gels or penetrating needles provide important, system-level demonstrations (fig. S4A and movie S2) (27). All materials that come into direct contact with the skin (Au, PI, and polyester) are biocompatible (30, 31). Measurements involved continuous use for as many as 6 hours. Devices worn for up to 24 hours or more on the arm, neck, forehead, cheek, and chin showed no degradation or irritation to the skin (figs. S14 and S15). Devices mounted in challenging areas such as the elbow fractured and/or debonded under full-range motion (fig. S16). ECG recordings from the chest (27) revealed

high-quality signals with information on all phases of the heartbeat, including rapid depolarization of the cardiac wave, and the associated QRS complex (Fig. 4A, right) (32). EMG measured on the leg (27) with muscle contractions to simulate walking and resting are presented in Fig. 4B, left. The measurements agree remarkably well with signals simultaneously collected using commercial, bulk tin electrodes that require conductive gels, mounted with tapes at the same location (Fig. 4B, right, and fig. S4B, right). An alternative way to view the data (spectrogram) is shown in Fig. 4C, in which the spectral content appears in a color contour plot with frequency and time along the y and x axes, respectively. Each muscle contraction corresponds
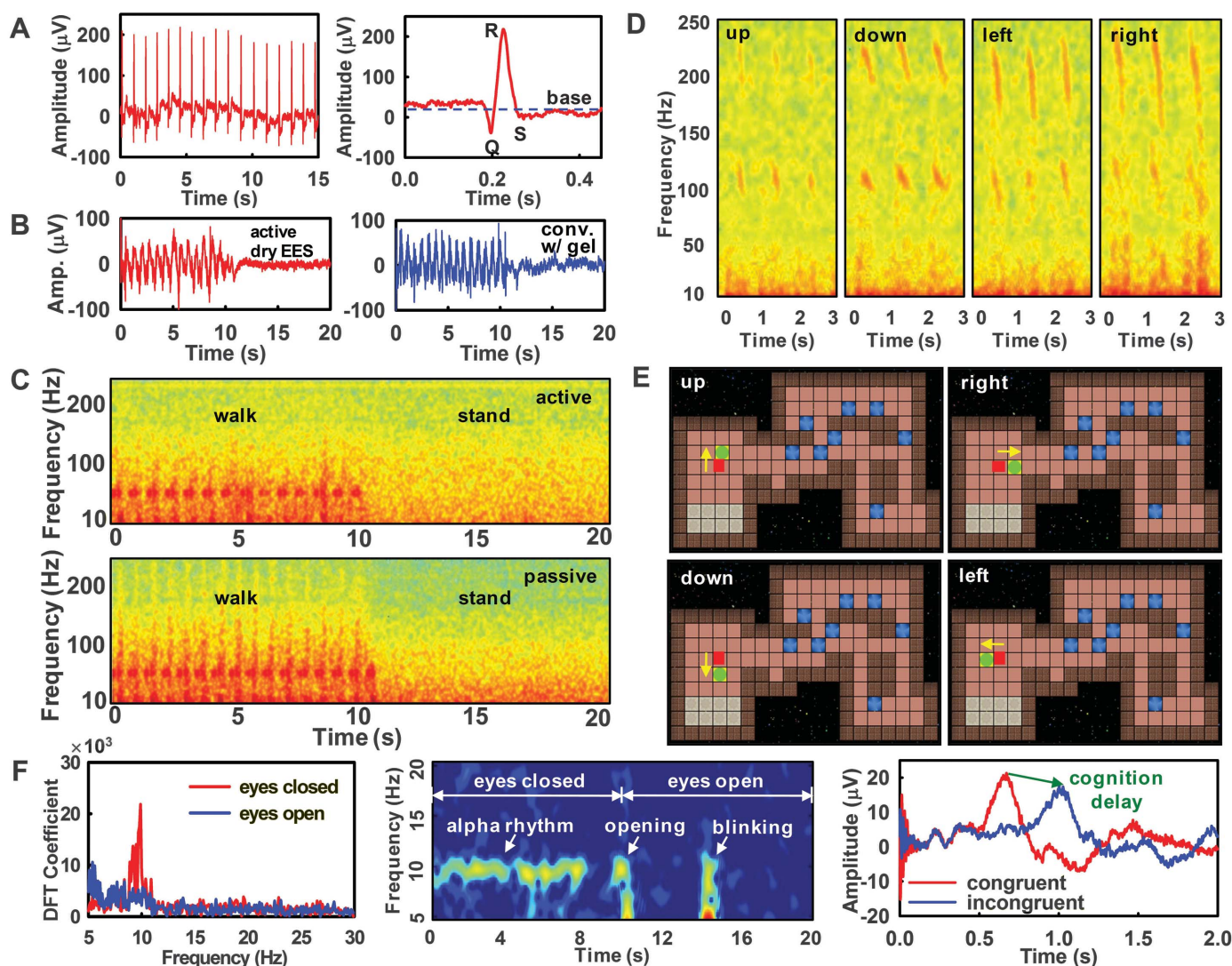

Fig. 4. (**A**) ECG signals measured with an active EES attached to the chest (left), and magnified view of data corresponding to a single heartbeat (right). (**B**) (Left) EMG measurements using an active EES, mounted on the right leg during simulated walking (from 0 to 10 s) and standing (from 10 to 20 s). (Right) Recordings collected with conventional sensors and conductive gel. (**C**) Spectrogram of the data in (B) for corresponding electrode type. (**D**) EMG spectrograms measured using an active EES mounted on the neck during vocalization of four different words: "up," "down," "left," and "right." (**E**) Simulated video game control by pattern recognition on EMG data from (D). The player icon is moved from an initial position (red) to destination (green). (**F**) (Left) Discrete Fourier transform (DFT) coefficients of EEG alpha rhythms at ~10 Hz (27), measured with a passive EES. (Center) The spectrogram of the alpha rhythm. The first and next 10 s correspond to periods when the eyes were closed and open, respectively. The responses at ~10 and ~14 s correspond to eye opening and blinking, respectively. (Right) Demonstration of Stroop effects in EEG measured with a passive EES.

to a red, vertical stripe that spans from 10 to 300 Hz (*32*).

To demonstrate EMG recording in a mode in which conventional devices are particularly ill suited, an EES mounted on the throat can monitor muscle activity, noninvasively, during speech (fig. S5A) (*27*). Here, recordings collected during vocalization of four words ("up," "down," "left," and "right"), repeated 10 times each (fig. S6) exhibit distinctive patterns, as in Fig. 4D. Measurements from another set of words ("go," "stop," and "great") (figs. S5B and S7) suggest sufficient structure in the signals for recognizing a vocabulary of words. These capabilities create opportunities for EES-based human/machine interfaces. As an example, dynamic time-warping pattern-recognition algorithms applied to throat-based EMG data (Fig. 4D) enable control of a computer strategy game (Sokoban), as illustrated in Fig. 4E. The classifications occur in less than 3 s on a dual-core personal computer running codes in MATLAB (MathWorks, Natick, MA), with an accuracy of >90% (fig. S8).

As a human/machine interface, EEG data offer additional promise. EES mounted on a region of the forehead that is first prepared by exfoliating the stratum corneum with Scotch tape yields reproducible, high-quality results, as demonstrated in alpha rhythms recorded from awake subjects with their eyes closed (fig. S9A) (*27*). The expected feature at ~10 Hz appears clearly in the Fourier-transformed data of Fig. 4F, left. The spectrogram of Fig. 4F, center, shows similar signatures. This activity disappears when the eyes are open. The signal-to-noise ratios are comparable with those obtained in otherwise identical experiments that used conventional, rigid bulk electrodes with conductive coupling gels. In further demonstrations, EEG measured with EES reveals well-known cognitive phenomena such as the Stroop effect (*33*, *34*). In these experiments, subjects randomly presented with congruent or incongruent (fig. S9B) colored words whisper the color (not the word) as quickly as possible. The data show that the motor responses pertaining to the whispering are manifested by two peaks at ~650 ms (congruent case) and ~1000 ms (incongruent case), as shown in Fig. 4F, right. The time delay implies that the congruent stimuli require fewer cognitive resources and are quicker to process than are the incongruent ones, which is consistent with the literature (*33*, *34*).

Conclusions. The materials and mechanics ideas presented here enable intimate, mechanically "invisible," tight and reliable attachment of high-performance electronic functionality with the surface of the skin in ways that bypass limitations of previous approaches. Many of the EES concepts are fully compatible with small-scale integrated circuits that can be released from ultrathin-body silicon-on-wafer substrates. For long-term use, materials and device strategies to accommodate the continuous efflux of dead cells from the surface of the skin and the processes of transpiration will be needed.

References and Notes
1. H. Berger, *Arch. Psychiatr. Nervenkr.* **87**, 527 (1929).
2. C. D. Hardyck, L. F. Petrinovich, D. W. Ellsworth, *Science* **154**, 1467 (1966).
3. E. J. Fox, R. Melzack, *Pain* **2**, 141 (1976).
4. J. G. Webster, Ed., *Medical Instrumentation: Application and Design* (Wiley, New York, 2009), pp. 189–240.
5. A. Searle, L. Kirkup, *Physiol. Meas.* **21**, 271 (2000).
6. P. Griss, H. K. Tolvanen-Laakso, P. Meriläinen, G. Stemme, *IEEE Trans. Biomed. Eng.* **49**, 597 (2002).
7. L. M. Yu, F. E. H. Tay, D. G. Guo, L. Xu, K. L. Yap, *Sens. Actuators A Phys.* **151**, 17 (2009).
8. B. Gerdle, S. Karlsson, S. Day, M. Djupsjöbacka, in *Modern Techniques in Neuroscience*, U. Windhorst, H. Johansson, Eds. (Springer Verlag, Berlin, 1999), pp. 705–755.
9. J. R. Ives, S. M. Mirsattari, D. Jones, *Clin. Neurophysiol.* **118**, 1633 (2007).
10. T. Sekitani *et al.*, *Science* **321**, 1468 (2008).
11. S. C. B. Mannsfeld *et al.*, *Nat. Mater.* **9**, 859 (2010).
12. K. Takei *et al.*, *Nat. Mater.* **9**, 821 (2010).
13. D.-H. Kim *et al.*, *Science* **320**, 507 (2008).
14. R.-H. Kim *et al.*, *Nat. Mater.* **9**, 929 (2010).
15. M. Kubo *et al.*, *Adv. Mater. (Deerfield Beach Fla.)* **22**, 2749 (2010).
16. M. Gonzaleza *et al.*, *Microelectron. Reliab.* **48**, 825 (2008).
17. S. P. Lacour, J. Jones, S. Wagner, T. Li, Z. Suo, *Proc. IEEE* **93**, 1459 (2005).
18. C. Keplinger, M. Kaltenbrunner, N. Arnold, S. Bauer, *Proc. Natl. Acad. Sci. U.S.A.* **107**, 4505 (2010).
19. L. Hu *et al.*, *Nano Lett.* **10**, 708 (2010).
20. O. Kuwazuru, J. Saothong, N. Yoshikawa, *Med. Eng. Phys.* **30**, 516 (2008).
21. M. Geerligs *et al.*, *J. Biomech.* **44**, 1176 (2011).
22. C. Pailler-Mattei, S. Bec, H. Zahouani, *Med. Eng. Phys.* **30**, 599 (2008).
23. http://dermatology.about.com/cs/skinanatomy/a/anatomy.
24. V. Arumugam, M. D. Naresh, R. Sanjeevi, *J. Biosci.* **19**, 307 (1994).
25. L. Tchvialeva *et al.*, in *Skin Roughness Assessment. New Developments in Biomedical Engineering*, D. Campolo, Ed. (InTech, www.intechopen.com/download/pdf/pdfs_id/9090, 2010).
26. K.-P. Wilhelm, P. Elsner, E. Berardesca, *Bioengineering of the Skin: Skin Surface Imaging and Analysis* (CRC, Boca Raton, 1997).
27. Materials and methods are available as supporting material on *Science* Online.
28. D.-H. Kim *et al.*, *Proc. Natl. Acad. Sci. U.S.A.* **105**, 18675 (2008).
29. A. Kaneko, N. Asai, T. Kanda, *J. Hand Ther.* **18**, 421, quiz 425 (2005).
30. K. C. Cheung, P. Renaud, H. Tanila, K. Djupsund, *Biosens. Bioelectron.* **22**, 1783 (2007).
31. M. Irimia-Vladu *et al.*, *Adv. Funct. Mater.* **20**, 4069 (2010).
32. L. Sörnmo, P. Laguna, *Bioelectrical Signal Processing in Cardiac and Neurological Applications* (Elsevier, Amsterdam, 2005).
33. J. R. Stroop, *J. Exp. Psychol.* **18**, 643 (1935).
34. O. Spreen, E. A. Strauss, *Compendium of Neuropsychological Tests: Administration, Norms and Commentary* (Oxford Univ. Press, New York, 2006).

A Highly Conserved Neutralizing Epitope on Group 2 Influenza A Viruses

Damian C. Ekiert,[1]* Robert H. E. Friesen,[2]* Gira Bhabha,[1] Ted Kwaks,[2] Mandy Jongeneelen,[2] Wenli Yu,[1] Carla Ophorst,[2] Freek Cox,[2] Hans J.W.M. Korse,[2] Boerries Brandenburg,[2] Ronald Vogels,[2] Just P.J. Brakenhoff,[2] Ronald Kompier,[2]† Martin H. Koldijk,[2] Lisette A.H.M. Cornelissen,[3] Leo L. M. Poon,[4] Malik Peiris,[4] Wouter Koudstaal,[2]‡ Ian A. Wilson,[1,5]‡ Jaap Goudsmit[2]

Current flu vaccines provide only limited coverage against seasonal strains of influenza viruses. The identification of V_H1-69 antibodies that broadly neutralize almost all influenza A group 1 viruses constituted a breakthrough in the influenza field. Here, we report the isolation and characterization of a human monoclonal antibody CR8020 with broad neutralizing activity against most group 2 viruses, including H3N2 and H7N7, which cause severe human infection. The crystal structure of Fab CR8020 with the 1968 pandemic H3 hemagglutinin (HA) reveals a highly conserved epitope in the HA stalk distinct from the epitope recognized by the V_H1-69 group 1 antibodies. Thus, a cocktail of two antibodies may be sufficient to neutralize most influenza A subtypes and, hence, enable development of a universal flu vaccine and broad-spectrum antibody therapies.

Influenza viruses cause millions of cases of severe illness each year, thousands of deaths, and considerable economic losses. Currently, two main countermeasures are used against flu. First, small-molecule inhibitors of the neuraminidase surface glycoprotein and the viral ion channel M2 have been widely used and proven to be quite effective against susceptible strains (*1*). However, resistance to these antivirals has reduced their effectiveness, and mutations associated with oseltamivir and amantadine are widespread (*2–4*). The second main countermeasure is vaccination. Current vaccines that are based on inactivated viruses elicit a potent immune response

ERRATUM

Post date 23 September 2011

Research Articles: "Epidermal electronics" by D.-H. Kim *et al.* (12 August, p. 838). In the first sentence of "Materials, mechanics, and design strategies" on p. 838, the substrate material was incorrectly identified. The end of that sentence should read, "...all integrated on the surface of a thin (~30 μm), gas-permeable elastomeric sheet based on a modified silicone (Smooth-on, Easton, USA) with low Young's modulus (~60 kPa) (fig. S1A)."